Dalton Transactions

ROYAL SOCIETY OF CHEMISTRY

PAPER

View Article Online
View Journal | View Issue

Cite this: *Dalton Trans.*, 2023, **52**, 9952

Effect of metal complexation on the radiolytic stability of DOTA†

Ilyes Mahti, Dominique Guillaumont, * Claude Berthon, Georges Saint-Louis, Xavier Hérès and Laurence Berthon *

Received 30th March 2023,
Accepted 24th June 2023

DOI: 10.1039/d3dt00977g

rsc.li/dalton

Radiometals are increasingly used in nuclear medicine for both diagnostic and therapeutic purposes. The DOTA ligand (1,4,7,10-tetraazacyclododecane-1,4,7,10-tetraacetic acid) is widely used as a chelating agent for various radionuclides, including ^{89}Zr, with high thermodynamic stability constants and great *in vivo* stability. However, in contact with radioisotopes, chelating molecules are subjected to the effects of radiation, which can lead to structural degradation and induce alteration of their complexing properties. For the first time, the radiolytic stability of the Zr–DOTA complex in aqueous solution was studied and compared to the stability of the DOTA ligand. The identification of the major degradation products allows us to propose two different degradation schemes for the DOTA ligand and Zr–DOTA complex. DOTA is degraded preferentially by decarboxylation and cleavage of an acetate arm CH_2–COOH, whereas in Zr–DOTA, DOTA tends to oxidize by the addition of the OH group in its structure. In addition, the degradation of the ligand, when involved in a Zr complex, is significantly less than when the ligand is free in solution, indicating that the metal protects the ligand from degradation. DFT calculations were performed to supplement the experimental data and give an improved understanding of the behaviour of DOTA and Zr–DOTA solutions after irradiation: the increase in stability upon complexation is attributed to the strengthening of the bonds in the presence of metal cations, which become less vulnerable to radical attack. Bond dissociation energies and Fukui indices are shown to be useful descriptors to estimate the most vulnerable sites of the ligand and to predict the protective effect of the complexation.

Introduction

Radiometals (or radionuclides) play an important role in nuclear medicine through imaging techniques to visualize the distribution of radionuclides in the body or through therapy by specific irradiation of malignant cells. Whatever the application, a pharmaceutical agent (drug) is needed to act as a carrier molecule to deliver radionuclides to the target. Metal-based radiopharmaceuticals represent a dynamic and rapidly expanding field of research. SPECT (Single Photon Emission Computed Tomography) and PET (Positron Emission Tomography) have become increasingly popular cancer imaging techniques. The development of clinical PET imaging has significantly increased the efficiency of cancer diagnosis.[1] For such PET applications, the ideal radionuclide emits β^+ particles and must have a short half-life with rapid accumulation and clearance in tissue. These radiopharmaceuticals provide imaging within 24 hours of administration. In this context, ^{89}Zr is currently being studied for PET[2–12] applications and has received considerable attention in radioimmunotherapy applications because of its favourable decay characteristics and half-life period ($t_{1/2}$ = 78.4 h) making it useful for labelling monoclonal antibodies.[13] To deliver ^{89}Zr to a given target, a powerful chelator must be bound to the tetravalent metal ion to prevent the release of the radionuclide into the human body.[14–16] The coordination chemistry of zirconium(IV) suggests the use of a polydentate ligand with a denticity of 6–8 oxygen and nitrogen donor atoms. Several families of ligands based on hydroxamate, hydroxypyridone, catecholamide, hydroxyisophthalimide or carboxylate donor groups have been investigated.[6,17] The desferrioxamine ligand (DFO) based on the hydroxamate donor group is the reference compound and is widely used in PET imaging.[18,19] However, with this ligand, a slight release of ^{89}Zr activity has been observed into the bones of mice.[4,20] This instability may be related to the unsaturated coordination sphere of Zr when complexed with DFO. Summers *et al.* reported that the coordination sphere of Zr complexed to DFO is likely completed by two hydroxide ligands, Zr(DFO)$(OH)_2$.[19]

Polyaminocarboxylic ligands, known for their high affinity for metal ions and strong binding ability to a wide range of

CEA, DES, ISEC, DMRC, Univ Montpellier, Marcoule, France.
E-mail: laurence.berthon@cea.fr, dominique.guillaumont@cea.fr

† Electronic supplementary information (ESI) available. See DOI: https://doi.org/10.1039/d3dt00977g

metal ions,[21,22] represent a class of ligands that has been at the forefront of radiopharmaceutical development for nearly half a century.[18,23–26] Pandya *et al.* used tetraazamacrocycles such as 1,4,7,10-tetraazacyclododecane-1,4,7,10-tetraacetic acid (DOTA) (Fig. 1) as a Zr chelator.[27] It was found that Zr–DOTA exhibited improved *in vitro* stability and *in vivo* behaviour compared to Zr–DFO. The molecular structure of Zr–DOTA was elucidated by single-crystal X-ray diffraction analysis and it was shown that Zr has an octodentate coordination with all four macrocyclic nitrogen atoms and acetate arms involved in the coordination.[27]

^{89}Zr decays to metastable ^{89m}Y by a combination of β^+ emission (23%) at low average energy ($E_{\beta^+} \approx 396$ keV) and electron capture (77%). ^{89m}Y undergoes an internal transition, which is accompanied by a high-energy (909 keV) gamma emission (99%) to give stable ^{89}Y.

In contact with radiometals, the chelator can be subjected to radiolysis attacks, which affect its chemical structure and lead to radiolytic decomposition. This phenomenon is of major concern as it can lead to the release of radiometals into the body.

Some works have reported the impact of irradiation on polyaminocarboxylic acid molecules such as EDTA, HEDTA or DTPA.[28–31] In the presence of ionizing radiation, these ligands in water are susceptible to indirect radiolysis and can be attacked by reactive species such as $H^\bullet$ and $HO^\bullet$ radicals.[32–35] Very few studies are available on DOTA radiolysis.[36,37] The alpha radiolysis of DOTA was investigated in aqueous solution under helium ion irradiation. This led to the formation of molecular hydrogen (H_2) and carbon dioxide (CO_2). It was observed that DOTA is degraded preferentially by decarboxylation (cleavage of CO_2 moieties), loss of acetate arms (CH_2COOH), and condensation of two carboxylic moieties with the elimination of a carbonic acid or glycolic acid group. In a recent study, Avraham *et al.* investigated the chemical reactions and changes that DOTA can undergo in response to radicals formed by the ionizing radiation induced by the radiometal.[37] The reaction of DOTA with $HO^\bullet$, $H_3C^\bullet$ and $H_3CO_2^\bullet$ radicals was investigated. Hydroxyl radicals were shown to react significantly faster than methyl radicals.[37] The authors have also studied the reactivity of lanthanide–DOTA complexes with methyl and hydroxyl radicals. It was shown that the methyl radical $H_3C^\bullet$ reacts more slowly with Ce^{III}–$DOTA^-$ and Dy^{III}–$DOTA^-$ complexes than with the free DOTA ligand. Such influence of metal ions on ligand radiolytic degradation, favouring or inhibiting certain reaction pathways, has already been observed in research work on solvent extraction for nuclear fuel reprocessing.[38–40] For instance, the effect of metal complexation on the reaction kinetics of the dodecane radical cation toward nuclear fuel extraction ligands was reported. Uranyl complexation increases the reaction rate with some amide type extracting ligands, while it has a negligible effect with tri-butyl phosphate ligand.[38] The complexation of americium and europium increases the reaction rate with the hexa-*n*-octylnitrilo-triacetamide ligand (HONTA).[39] Kimberlin *et al.* characterized the effect of lanthanide complexation on the radiolysis of diglycolamide, finding that metal ions protect diglycolamide from degradation.[40] Other studies have investigated the effect of metal complexation in aqueous solution.[30,41–49] For example, in the case of DTPA solution, it was observed that the radiolytic yield of degradation was higher for uncomplexed DTPA than for the Sm–DTPA complex.[50] These results underline the importance of considering the role of metals in radiolysis even though the effect of metal complexation on ligand radiolysis remains poorly understood. Recent work has shown that quantum chemistry tools can be very useful to complement experimental data in the study of radiolytic processes. In particular, Fukui functions and bond dissociation energies (BDEs) have been used to explain differences in the behaviour of ligands under irradiation.[40,51–55] Fukui indices evaluate the chemical reactivity of a particular atom towards electrophilic, nucleophilic or radical attack, while BDEs assess bond strength. These tools allow the identification of the weak points of the molecules and thus the identification of the atoms susceptible to radiolysis attacks.

The goal of this work is to study the radiolytic stability of the DOTA ligand and Zr–DOTA complex in water to investigate the influence of complexation on the radiolytic stability of DOTA. Gamma irradiations were performed as the high-energy gamma emission of the ^{89m}Y decay is the major concern of ^{89}Zr decay chain. The degradation products of DOTA and the Zr–DOTA complex have been identified and degradation schemes are proposed. Finally, bond stabilities and Fukui functions have been determined from DFT calculations in order to evaluate the most likely sites for radical attack on the ligand and the effect of complexation.

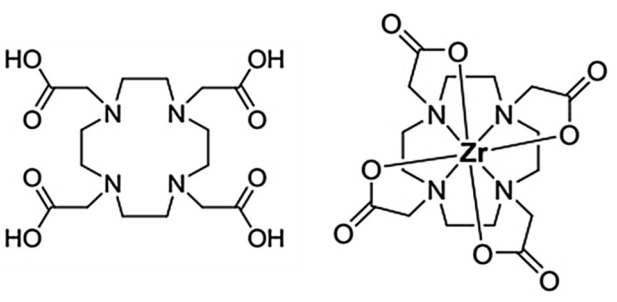

Fig. 1 Schematic representation of the DOTA ligand (left) and Zr–DOTA complex (right). For simplicity's sake, DOTA is portrayed as neutral form regardless of the proton position.

Experimental section

Chemicals

Solid DOTA (H_4DOTA) was purchased from Chematech (Dijon, France) (purity > 98%, confirmed by HPLC). Solid zirconium (IV) acetylacetonate was obtained from Sigma-Aldrich (purity 97%). Anhydride methanol from Sigma-Aldrich (purity 99.8%) was utilized. All commercial products were used as received without further purification. The pH of the solutions was

measured with a pH electrode (Metrohm) calibrated against standard buffers.

Synthesis and characterization of Zr–DOTA

The Zr–DOTA complex was synthesized at room temperature and with a metal : ligand ratio of 1 : 1. 203 mg of solid DOTA (H_4DOTA) was dissolved in methanol. DOTA did not dissolve completely after stirring. $Zr(AcAc)_4$ was then slowly added to the solution. The resulting mixture was centrifuged and the supernatant was isolated in a separate microtube. After a few days, a precipitate appeared, which was separated and dried. Finally, a white powder corresponding to Zr–DOTA was obtained which was dissolved in pure water for characterization by mass spectrometry and NMR spectroscopy. The spectra are presented in the ESI.†

Irradiation experiments

Aqueous solutions of DOTA and Zr–DOTA (5×10^{-3} mol L^{-1}) were irradiated by gamma radiation using a GRS-D1 Gamma-Service-Medical-GmbH irradiation system at CEA Marcoule. It uses a calibrated ^{137}Cs source with a dose rate of 0.8–0.9 kGy h^{-1}. Dosimetry was performed by the Fricke method.[56]

The concentration of ^{89}Zr used for *in vivo* studies is approximately 1–2 × 10^{-7} M, which corresponds to a maximum dose rate of 0.3 kGy h^{-1} (without taking into account zirconium decay).[27,57] Considering the position of the samples in the gamma irradiator, the dose rate delivered to the samples is three times higher. Under these conditions, degradation products are formed more rapidly than under usual *in vivo* conditions. However, to compare the effect of complexation on DOTA stability, all samples were irradiated under identical experimental conditions (DOTA concentration, irradiation dose and dose rate).

2 mL of each sample was prepared and irradiated for 12–24–36–120 hours corresponding to a dose of approximately 10–20–30–100 kGy. The doses, corresponding irradiation times and pH of the irradiated samples are given in Table 1.

Mass spectrometry

The samples were diluted in a concentration range of 10^{-4}–10^{-3} mol L^{-1} in pure H_2O or acidified water (H_2O + 0.02%$_{Vol}$ HNO_3) and analyzed with a micrOTOF-Q II (Bruker Daltonik GmbH, Bremen, Germany) electro-spray ionization (ESI) quadrupole time-of-flight (TOF) mass spectrometer calibrated daily using an Agilent (G1969-85000) ESI Low Concentration Tuning Solution. The addition of acid favours ionization of compounds and avoids the formation of sodium adducts. No other effects of the acid were observed. The samples were injected at a flow rate of 300 μL h^{-1} by using a syringe pump. The experimental conditions were as follows: positive ion mode, ion spray voltage of −4500 V, IsCID 0 eV, N_2 as the drying and nebulizing gas, 4 L min^{-1}, 0.3 bar, and 200 °C. A low mass tuning method was used, which allowed the analysis of DOTA and Zr–DOTA fragments. The Compass Data Analysis software (Bruker Daltonik) was used for data processing. Species were identified by comparing an experimental isotopic pattern with a simulated one using the DataAnalysis 4.2 software. MS/MS analysis of DOTA and major degradation products is given in the ESI.†

Table 1 Dose rate, irradiation time, doses and pH of the samples

Sample	Dose rate (kGy h^{-1})	Irradiation time (h)	Dose (kGy)	pH
DOTA 0 kGy	0	0	0	3.51
DOTA 10 kGy	0.87	9 h 25	8.2	3.82
DOTA 20 kGy	0.86	23 h	20	4.22
DOTA 30 kGy	0.87	38 h 25	34	4.51
DOTA 100 kGy	0.87	120 h	104	—
Zr–DOTA 0 kGy	0	0	0	5.7
Zr–DOTA 10 kGy	0.80	10 h 25	8.3	3.44
Zr–DOTA 20 kGy	0.80	25 h	20	3.37
Zr–DOTA 30 kGy	0.80	38 h 25	31	3.39
Zr–DOTA 100 kGy	0.87	120 h	104	—

Nuclear magnetic resonance

Analyses were performed at 25 °C with an Agilent DD2 400 MHz spectrometer equipped with a 5 mm OneNMR probe. To avoid dilution, an external tube containing the deuterated reference solvent ($CDCl_3$ or acetoneD6) surrounded the tube containing the sample in pure H_2O. All spectra were normalized with the reference solvent used as the external standard.

The ^{1}H NMR water signal was presaturated to enhance the signal intensity of our compounds. The OpenVnmrJ 4.2 software was used for data acquisition and the MestReNova 14.2.1 software for data processing.

Computational methods

The calculations were performed using density functional theory (DFT) with Gaussian 16.[58] Optimized geometries were confirmed to be true minima by frequency calculations (no imaginary frequencies were found). The zero-point energies (ZPE) with the corresponding thermal correction at 298.15 K were computed by frequency calculations and added to the electronic energies. The 6-31G+(d,p) basis set was employed for H, C, N and O atoms. For zirconium, core electrons were represented by the MWB28 Stuttgart-Cologne quasi-relativistic effective core potential (ECP) with the associated basis set for valence electrons.[59] The bond dissociation energy (BDE) is defined as the reaction enthalpy of homolytic bond dissociation according to the following reaction:

$$\mathrm{R{-}X} \rightarrow \mathrm{R^{\bullet}} + \mathrm{X^{\bullet}} \quad (1)$$

The BDE of an R–X bond is calculated by using the difference in the enthalpies of each species involved in the homolytic reaction.

$$E_{\mathrm{BDE}} = \Delta_f H^{\circ}_{298.15\,\mathrm{K}}(\mathrm{R^{\bullet}}) + \Delta_f H^{\circ}_{298.15\,\mathrm{K}}(\mathrm{X^{\bullet}}) - \Delta_f H^{\circ}_{298.15K}(\mathrm{R-X}) \quad (2)$$

The hybrid density functional B3P86 (Becke's 3-parameter exchange functional with Perdew non-local correlation

energy)[60,61] was chosen to compute BDEs. Previous studies have shown good agreement with the experimental values for compounds similar to the acetate arm of DOTA, *i.e.* containing C–N, C–O or C–C bonds.[62–64] It has been shown that B3P86 has an absolute mean error of 10.8 kJ mol^{-1}, while B3LYP has an absolute mean error of 27 kJ mol^{-1} for such bonds. All BDE calculations were performed in the gas phase.

The Fukui function as defined by Parr and Yang[65] describes the electron density at a given position r after adding or removing electrons. It can predict the sites of a molecule which are most likely to undergo a nucleophilic, electrophilic or radical attack. In this work, the Fukui function R for radical attack has been determined. It corresponds to:

$$R(r) = \frac{1}{2}\left[\rho_{N+1}(r) - \rho_{N-1}(r)\right] \quad (3)$$

ρ is the electronic density and N is the number of electrons. $\rho_{N+1}(r)$ is the electronic density of the anion generated from adding one electron to $\rho_N(r)$, density of the neutral molecule. $\rho_{N-1}(r)$ is the electronic density of the cation generated by removing an electron from $\rho_N(r)$. Positive values of these functions indicate which parts of the molecule are most vulnerable to radical attack. On the opposite, negative values would indicate which parts of the molecule are unlikely to be attacked by such species.

The Fukui indices have also been generated to obtain a quantitative description of the local reactivity.[53,55] The radical Fukui index $f^{0,\alpha}$ for an atom α is defined as follows:

$$f^{0,\alpha} = \frac{1}{2}\left[q^{\alpha}_{N-1} - q^{\alpha}_{N+1}\right] \quad (4)$$

where q^{α} is the partial charge on the atom α.

Finally, the condensed dual descriptor (CDD) proposed by Morell *et al.*[66,67] was determined. It provides useful information on both stabilizing and destabilizing nucleophile/electrophile interactions and helps to identify the behaviour of a specific atom within a molecule. It corresponds to a linear combination of Fukui indices:

$$\mathrm{CDD}_{\alpha} = 2q^{\alpha}_{N} - q^{\alpha}_{N+1} - q^{\alpha}_{N-1} \quad (5)$$

The absolute value of CDD indicates the probability of the reaction with the site. The sign of CDD corresponds to the type of attack, and negative and positive values correspond, respectively, to nucleophilic and electrophilic attacks. For Fukui calculations, the geometries of DOTA and Zr–DOTA were optimized for the neutral reference using the B3LYP functional.[68,69] The water was represented with the self-consistent reaction field (SCRF) method using the polarizable continuum model (IEFPCM).[70] For Fukui indices and the condensed dual descriptor, the partial charges were derived from a natural population analysis (NBO).[71]

Results and discussion

Radiolytic stability of the free and complexed ligands

^{1}H NMR analysis of 5 mM DOTA and Zr–DOTA samples in pure water was performed before and after radiolysis up to 100 kGy. ^{1}H NMR spectra for the irradiated solutions up to 30 kGy are presented in Fig. 2 and 3. Their spectra were normalized using an external locking solvent so that the spectra can be compared with each other. An undeuterated residual signal from acetoneD6 for DOTA and a tetramethylsilane (TMS) signal in $CDCl_3$ for Zr–DOTA were observed. The spectra of the solution irradiated at 100 kGy were not presented because they were hardly usable. At 100 kGy, the NMR signals of Zr–DOTA and DOTA are strongly reduced and in the case of Zr–DOTA, a white powder was observed in the bottom of the Pyrex flask, indicating that some zirconium has been hydrolysed.

For the DOTA sample (pH of the solution before irradiation = 3.51), the characteristic signals of DOTA are observed at 2.26 ppm corresponding to the cyclen protons and at 2.74 ppm corresponding to the acetate protons (Fig. 2). From 10 kGy onwards, the signals of the acetate protons are shifted, indicating that the arms of DOTA are degraded, and some signals appear between 1 and 3 ppm. Another signal is also observed at 7.38 ppm. These signals can be attributed to the formation of degradation products. A decrease in signal intensity is observed upon irradiation, which was also reported by Fiegel *et al.*[36] They observed that the higher the concentration of DOTA in solution, the higher the hydrogen yields and attributed the decrease in NMR signal intensity to the degradation of DOTA through hydrogen abstraction leading to the formation of molecular hydrogen H_2.[36] At 20 and 30 kGy, DOTA keeps degrading. This results in a decrease in intensity and an increasing shift of the NMR signals. On the other hand, the signal intensity of degradation products increases slightly. At 30 kGy, the increasing number of signals is causing a broadening of the baseline from 1.5 to 3.1 ppm.

The ^{1}H NMR spectra of the irradiated solutions of Zr–DOTA (pH of the solution before irradiation = 5.7) are shown in Fig. 3. The pH was not equalized between the ligand and the complex solutions to avoid the effects of acidic or basic species on the radiolysis of the samples. Moreover, previous studies have shown that within the pH range from 3 to 11, in the case of gamma irradiation, the radiolytic yields of the main radiolysis products of water (e^-_{aq}, $HO^{\bullet}$, $H^{\bullet}$, H_2, H_2O_2 and $HO_2^{\bullet}$) barely change.[32] The characteristic signals of the complex are visible and are assigned according to the literature.[72] More details are provided in the ESI.† Zr–DOTA shows a different behaviour from that of the free ligand towards irradiation. As shown in Fig. 3, the signals of the complex are not shifted and their intensity hardly decreases. This indicates that the complex is more resistant to irradiation than the free ligand. Nonetheless, as for the free ligand, new signals appear upon irradiation but they are much less numerous.

The NMR signals of the ligand and complex were integrated between 0 and 30 kGy (see the ESI†). The average intensity of the signals decreases by 94% for DOTA and 42% for Zr–DOTA

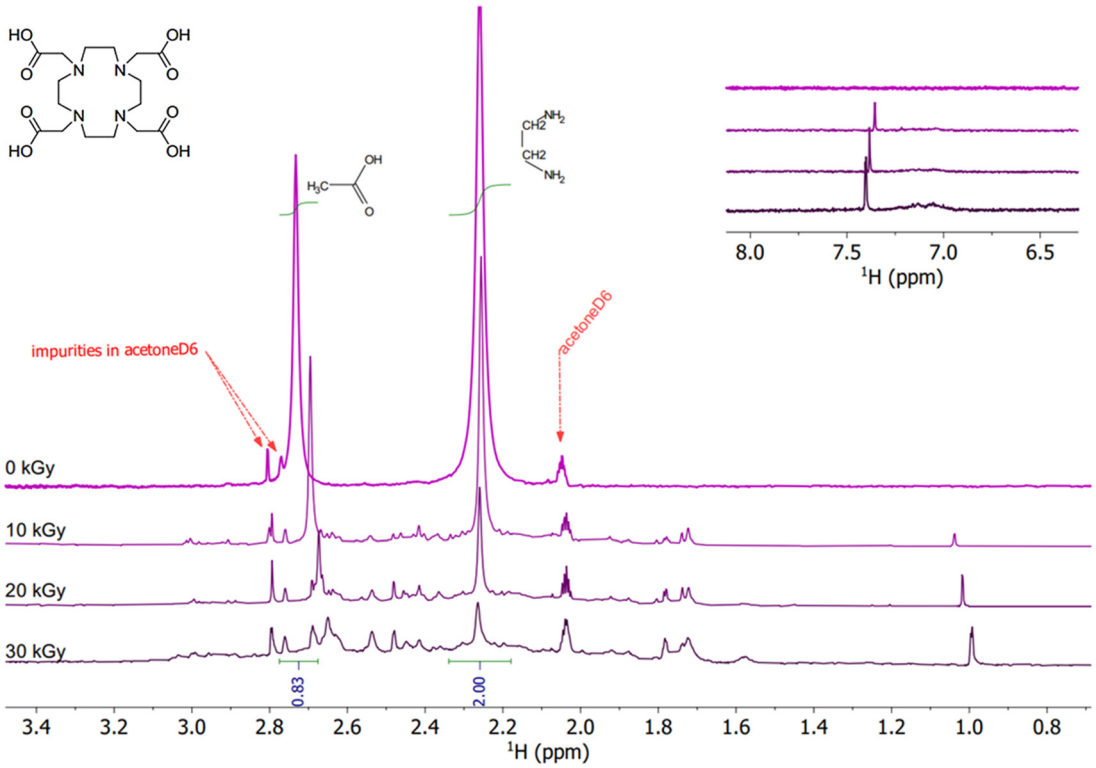

Fig. 2 ^{1}H NMR spectra of non-irradiated and irradiated DOTA solutions. Conditions: 5 mM in pure water (pH = 3.51). AcetoneD6 is used as an external lock solvent and residual undeuterated signal to normalize the spectra. From top to bottom: 0 kGy, 10 kGy, 20 kGy, and 30 kGy.

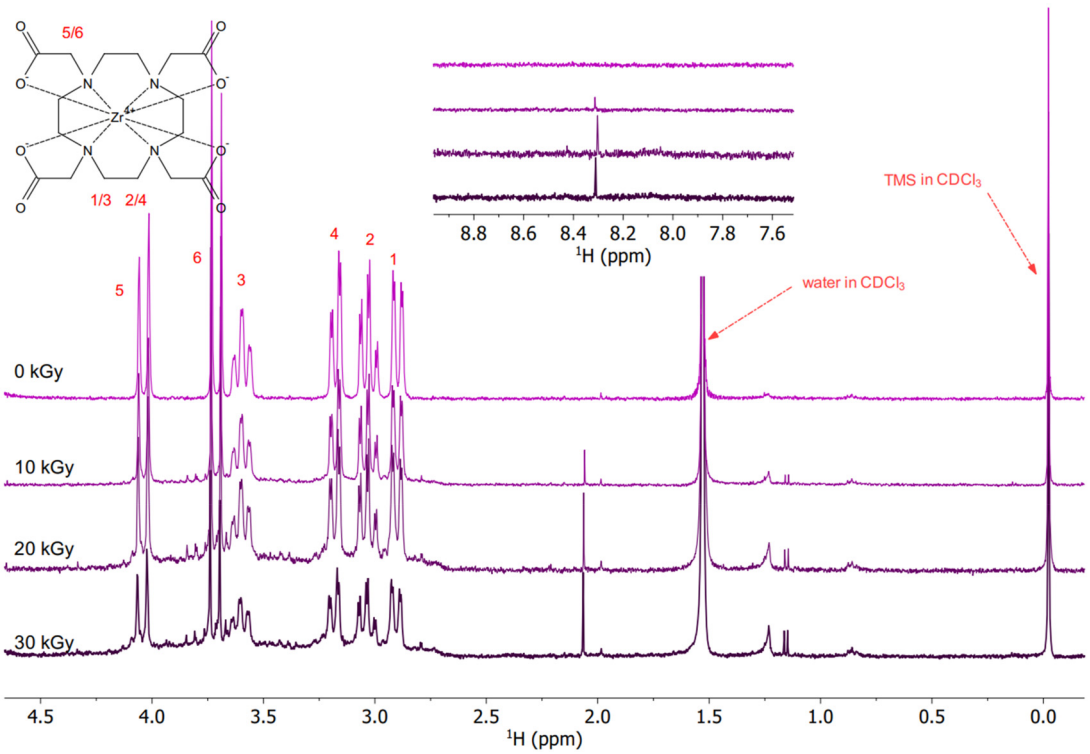

Fig. 3 ^{1}H NMR spectra of non-irradiated and irradiated Zr–DOTA solutions. Conditions: 5 mM in pure water (pH = 5.7). All spectra are normalized to the TMS present in external $CDCl_3$ used as the lock solvent. From top to bottom: 0 kGy, 10 kGy, 20 kGy, and 30 kGy.

Table 2 Dose constants (kGy^{-1}) and $-G_0$ values ($\mu mol\ J^{-1}$) for irradiated DOTA and Zr–DOTA

Sample	d (kGy^{-1})	$-G_0$ ($\mu mol\ J^{-1}$)
DOTA	−0.125 ± 0.003	0.625 ± 0.015
Zr–DOTA	−0.0193 ± 0.003	0.096 ± 0.015

at 30 kGy. Considering the exponential decrease in the DOTA concentration with absorbed dose, which suggests pseudo-first-order kinetics, the dose constants d and G_0 values can be calculated using eqn (6) and (7) from Mincher *et al.*[73,74] C_0 and C are the initial and final concentrations (the C/C_0 ratio was calculated using the NMR peak areas), ρ is the density of the solution and D is the absorbed dose. The results are given in Table 2. Notably, the values obtained for $-G_0$ (radiolytic yields of disappearance) are much lower when the ligand is complexed with zirconium.

$$C = C_0 e^{dD} \quad (6)$$

$$G_0 = dC_0/\rho \quad (7)$$

In summary, the degradation of the free ligand is much more pronounced than when complexed with Zr, considering the large decrease in intensity, $-G_0$ and the shift of the ligand signals for the DOTA solutions. Most importantly, the lower occurrence of new signals after irradiation of the complex indicates that fewer degradation products are generated with Zr. The metal seems to protect the ligand from degradation.

The solutions were then analysed by ESI-MS to identify the degradation products. Fig. 4 shows the ESI-MS spectra of the DOTA aqueous solutions irradiated up to 30 kGy. At 0 kGy, one species is observed at m/z = 405 corresponding to the protonated DOTA ligand. From 10 to 30 kGy, peaks corresponding to the degradation products of DOTA are observed at m/z = 347, 317 and 361. The identifications were proposed based on the work of Fiegel *et al.*[36] The major ion at m/z = 347 corresponds to DOTA with the loss of an acetate arm $-CH_2COOH$. This explains the shift of the acetate arm signals observed in the NMR spectra. The two other ions are assigned to the loss of carbon dioxide groups, one molecule of CO_2 at m/z = 361 and two molecules of CO_2 at m/z = 317. The abundance of ions gradually decreases with the absorbed dose, causing ligand degradation as observed by NMR. An increase of the pH is also observed (Table 1), from 3.51 to 4.51, certainly due to the release of CO_2.

From the species identified by ESI-MS, a simplified degradation pathway of DOTA is proposed with the major degradation products (Fig. 5). This is in good agreement with the previous one proposed by Fiegel *et al.* However, fewer degradation products are detected, as the initial concentration is lower in the present study (5 mM *vs.* 100 mM in the study of Fiegel *et al.*).

The Zr–DOTA solutions were also analysed by ESI-MS (Fig. 6). A previous investigation has shown that ESI-MS is a valuable tool to identify metal–DOTA complexes in solution.[75] At 0 kGy, a species is observed at m/z = 491 and corresponds to

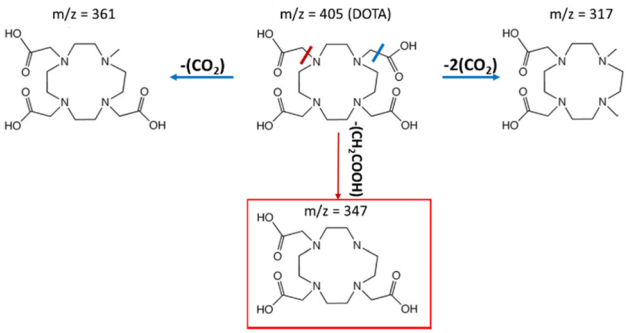

Fig. 5 Simplified degradation pathway for DOTA radiolysis in pure water. The compound framed in red is the major degradation product observed by ESI-MS.

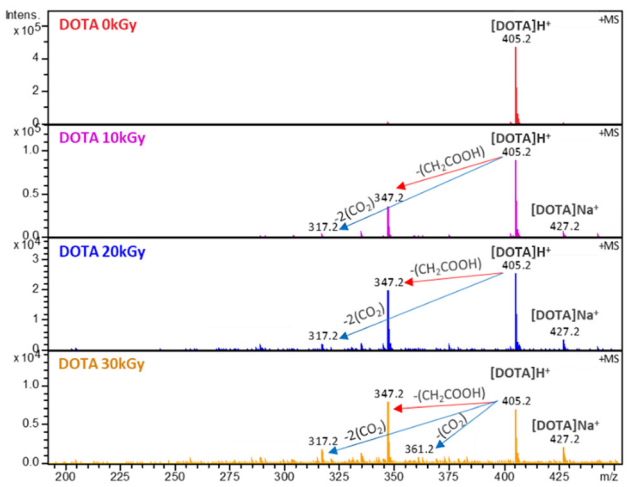

Fig. 4 ESI-MS spectra of degraded solutions of 5 mM DOTA diluted 10 times in acidified water (H_2O + 0.02%/Vol HNO_3). Positive ionization mode.

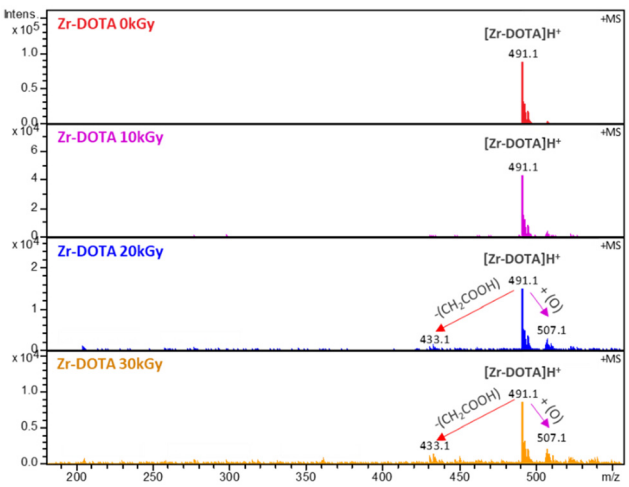

Fig. 6 ESI-MS spectra of degraded solutions of 5 mM Zr–DOTA diluted 10 times in acidified water (H_2O + 0.02%/Vol HNO_3). Positive ionization mode.

the protonated complex. In contrast to the free ligand, the abundance of degradation products is much lower. However, a degradation product is observed at a lower mass (m/z = 433). This compound results from the loss of a CH_2COOH fragment, as observed for the free ligand. Nevertheless, its signal intensity is weak, suggesting that it is present in small amounts. This decarboxylation has been previously observed with the aged solution of Ce–DOTA complexes.[76] It was attributed to the intramolecular and intermolecular redox processes. A heavier degradation product, not observed with free DOTA, is found at m/z = 507. The mass gain is 16 and may correspond to an addition of an oxygen atom to the complex. This can be attributed to C–H bond breaking, due to the reaction with the $H^{\bullet}$ radical from the solution, leading to the release of H_2 according to eqn (8). This could explain the small decrease in intensity of the NMR signals observed for the complex (Fig. 3). The dehydrogenated radical intermediate then reacts with a free $HO^{\bullet}$ radical as described in reaction (9):

$$RR'\,ZrNCH_2COOH + H^{\bullet} \rightarrow RR'\,ZrN -^{\bullet} CHCOOH + H_2 \quad (8)$$

$$RR'\,ZrN -^{\bullet} CHCOOH + HO^{\bullet} \rightarrow RR'\,ZrNCH(OH)COOH \quad (9)$$

In contrast, the gamma radiolysis of diglycolamide ligands in aqueous nitrate solution has been shown to be driven by the hydroxyl ion which reacts rapidly with the ligands.[77]

Therefore, unlike the ligand, the Zr–DOTA complex tends to oxidize under irradiation. Oxidation reactions have already been observed under certain conditions with amide extractants in organic diluents.[51,78,79] In summary, Zr–DOTA degrades differently from the free ligand. The results obtained by ESI-MS are in agreement with those obtained by ^{1}H NMR: fewer degradation products are observed for the complex. An instant decrease of the pH is observed (Table 1) for the complex from 5.7 to 3.4. This is probably due to the release of acetic acid and zirconium hydrolysis.

Fig. 7 shows a simplified degradation pathway for Zr–DOTA with the main degradation products observed by ESI-MS. MS/MS experiments were conducted on the degradation product at m/z = 507 to obtain further structural information. However, due to the very low abundance of the ion, it was not possible to observe enough fragments to identify precisely the structure. Thus, two degradation products are proposed, one by hydroxylation in the acetate arms and the other in the cyclen.

To summarize the results, the degradation products observed for DOTA and Zr–DOTA are shown in Table 3.

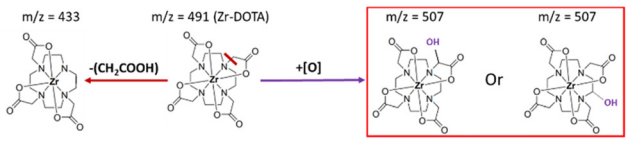

Fig. 7 Simplified degradation pathway for Zr–DOTA radiolysis in water. Compounds framed in red are the major degradation products observed by ESI-MS.

Table 3 Degradation products observed for DOTA and Zr–DOTA

m/z	Chemical formula	Species
DOTA		
405.2	$[C_{16}H_{28}O_8N_4]H^+$	DOTA
347.2	$[C_{14}H_{26}O_6N_4]H^+$	Loss of CH_2COOH
317.2	$[C_{14}H_{28}O_4N_4]H^+$	Loss of 2 CO_2
361.2	$[C_{15}H_{28}O_6N_4]H^+$	Loss of CO_2
Zr–DOTA complex		
491.2	$[ZrC_{16}H_{24}O_8N_4]H^+$	Zr–DOTA
507.1	$[ZrC_{16}H_{24}O_9N_4]H^+$	Addition of O
433.1	$[ZrC_{14}H_{26}O_6N_4]H^+$	Loss of CH_2COOH

Quantum chemistry calculations

In order to evaluate the strength of the bonds in DOTA, free or engaged with Zr, bond dissociation energies (BDEs) were evaluated from DFT calculations. The speciation of DOTA in water depends on the pH of the solution. From the previously determined protonation constants and identified protonation sites,[80–82] it is considered that the predominant species in aqueous solution at pH 3–4 has four protons attached to two *trans* nitrogen atoms of the ring and to two carboxylate groups as shown in Fig. 8. Calculations were performed for this species, which will be referred to as H_4DOTA hereafter.

Our experimental results and previous work[36] show that cyclen bonds of DOTA are not subjected to radiolysis, while the acetate arms can be broken. Therefore, BDEs were calculated only for the bonds belonging to the acetate arms. The BDEs corresponding to the N–C, C–C, C–O and C–H bonds depicted in Fig. 8 were computed for H_4DOTA and Zr–DOTA. The results are summarized in Table 4. The C–H BDE values are not discussed at first, as they are involved in degradation mechanisms as proved by previous authors for polyaminocarboxylic acids.[28,36]

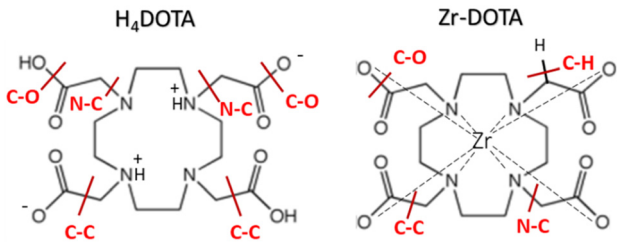

Fig. 8 Bonds studied for H_4DOTA and Zr–DOTA.

Table 4 Computed bond dissociation energies (BDEs in kJ mol^{-1}) for acetate arms of H_4DOTA and Zr–DOTA

	H_4DOTA		
R–X bond	Uncharged arm	Charged arm	Zr–DOTA
C–C	300	762	741
N–C	257	669	720
C–O	500	1078	1068
C–H	266	426	314

According to the calculated values for H_4DOTA, the lower value and therefore the weakest bond for any arms of H_4DOTA, with protonated and unprotonated nitrogen, corresponds to the N–C bond. Breaking this bond induces the loss of an acetate arm, CH_2COOH. This is consistent with the experimental data that give DOTA with a loss of CH_2COOH as the major degradation product. When comparing H_4DOTA and Zr–DOTA, the weakest bonds are found in H_4DOTA with BDE values ranging from 300 to 500 kJ mol^{-1} for the C–C, C–N and C–O bonds of uncharged arms. In Zr–DOTA, these values are significantly higher and vary from 720 to 1068 kJ mol^{-1}. This difference indicates that the bond stabilities of the acetate arms are greatly enhanced when the ligand is complexed with zirconium. This increase in stability upon complexation is also consistent with what has been observed experimentally. It should be mentioned that the BDE values of the charged arms of H_4DOTA are similar to those computed for Zr–DOTA (from 669 to 1078 kJ mol^{-1}). This shows that the BDEs, and hence the bond stability, are strongly influenced by the presence of a cation (either Zr^{4+} or H^+) attached to the ligand.

The calculated bond distances given in Table 5 indicate that there is no correlation between bond distances and BDE variations. For instance, the N–C bond distance is shorter in H_4DOTA for the uncharged arm than that in Zr–DOTA: 1.473 Å *vs.* 1.485 Å, while the BDE is lower (257 and 720 kJ mol^{-1} respectively).

The BDE value depends on the relative stability between the R–X molecule and the formed radicals R$^\bullet$ and X$^\bullet$ (eqn (2)). In the case of the HN^+–C bond of H_4DOTA, the cleavage of the bond leads to $RR'HN^{\bullet+}$ and $CH_2COO^{\bullet-}$ charged radicals. This bond is calculated to be more stable than the neutral N–C bond (669 *vs.* 257 kJ mol^{-1}). Previous studies have shown similar results for N–H bonds.[83–85] For example, Kaur *et al.* have found a BDE for protonated NH_3 of 514 kJ mol^{-1} whereas for the neutral form they found a BDE of 433 kJ mol^{-1}. According to our calculations, the protonation of RR′N$^\bullet$ stabilizes the radical product by 1032 kJ mol^{-1} whereas the deprotonation of $CH_2COOH^\bullet$ destabilizes the radical product by 1444 kJ mol^{-1}. This results in a decrease of the N–C BDE between the charged and the uncharged arm of 412 kJ mol^{-1}. These results indicate that the destabilization of $CH_2COO^{\bullet-}$ is responsible for the bond stabilization.

Finally, the lower BDE is found in Zr–DOTA for the C–H bonds in the acetate arms. This result corroborates the experimental degradation pathway observed for Zr–DOTA, *i.e.* oxidation to form Zr–DOTA[O] by replacing H$^\bullet$ for HO$^\bullet$ due to the rupture of a C–H bond. This phenomenon is not observed for H_4DOTA because the cleavage of the C–H bond is immediately followed by the rupture of C–C bonds or N–C bonds through multiple reactions and rearrangement.[28,36]

The Fukui function, Fukui indices and absolute values of the condensed dual descriptor were determined for H_4DOTA and Zr–DOTA. The Fukui function describes the electron density after the addition or removal of the electron. It can predict the sites of a molecule that are most likely to undergo nucleophilic, electrophilic or radical attack. The Fukui indices determined for individual atoms give access to local reactivity (see the Computational methods section). Fig. 9 shows the values of the radical Fukui functions mapped onto the electron density isosurface for H_4DOTA and Zr–DOTA. The higher the value, the more vulnerable the site is to radical attack (red dots).

For the ligand (H_4DOTA) and the complex (Zr–DOTA), the higher values of the radical Fukui function are located on the carboxylate groups around the oxygen atoms. As expected, the smaller values are found on the carbon cyclen (blue in Fig. 9). Furthermore, for H_4DOTA, the values of the radical Fukui function are higher for the unprotonated nitrogen atom (red dots) than for the protonated nitrogen atoms. For Zr–DOTA, no red dots are observed on nitrogen atoms. Other Fukui function values are also smaller on Zr–DOTA than those on DOTA, as shown by the predominant blue parts and fewer red dots in Fig. 9 (bottom view).

Afterwards, we calculated the radical Fukui indices (f^0) and absolute values of the condensed dual descriptor (|CDD|) for each atom to quantify the most reactive sites of the ligand and the complex. The f^0 and CDD values of the carbon atoms of H_4DOTA and Zr–DOTA are shown in Table 6. For clarity, only carbon and nitrogen Fukui indices are given. The complete list of the calculated values is given in the ESI.†

For Zr–DOTA, the lowest f^0 value is found for the cyclen carbon atoms ($C_{(CH_2,\ cyclen)}$) with a slightly negative average value of −0.004 indicating that they are not sensitive to radical attack. On the other hand, the highest values are obtained for carboxylate carbon atoms $C_{(COO^-)}$, which can be assimilated to the release of CO_2 due to the cleavage of the C–C bond. The values of the nitrogen and $C_{(CH_2,\ RN\ arm)}$ atoms are positive and suggest that the N–C bond is also prone to radical attack. The CDD values give the same indications, with high values for acetate carbon and nitrogen atoms and low values for cyclen carbon atoms. This also suggests that the oxidation of the complex, observed experimentally, occurs preferentially on the carboxylate arm rather than on the cyclen.

In the case of H_4DOTA, the highest values of f^0 are obtained for $C_{(COOH)}$, N and $C_{(CH_2,\ N\ arm)}$ (0.079, 0.049 and 0.012*e*), similarly to Zr–DOTA, and correspond to the atoms belonging to the acetate arms. Interestingly, these f^0 values correspond to the acetate arms with unprotonated nitrogen. When the nitrogen is protonated, the values are much lower for the same atoms. The same trend is observed for the CDD values. As for Zr–DOTA, the smallest f^0 values are determined for the cyclen carbon atoms and they are the only negative ones (−0.004*e*).

Table 5 Bond distances (Å) of acetate arms for optimized structures by DFT of H_4DOTA and Zr–DOTA

	H_4DOTA		
R–X bond	Uncharged arm	Charged arm	Zr–DOTA
C–C	1.536	1.554	1.528
N–C	1.473	1.502	1.485
C–O	1.306	1.278	1.309
C–H	1.095	1.092	1.093

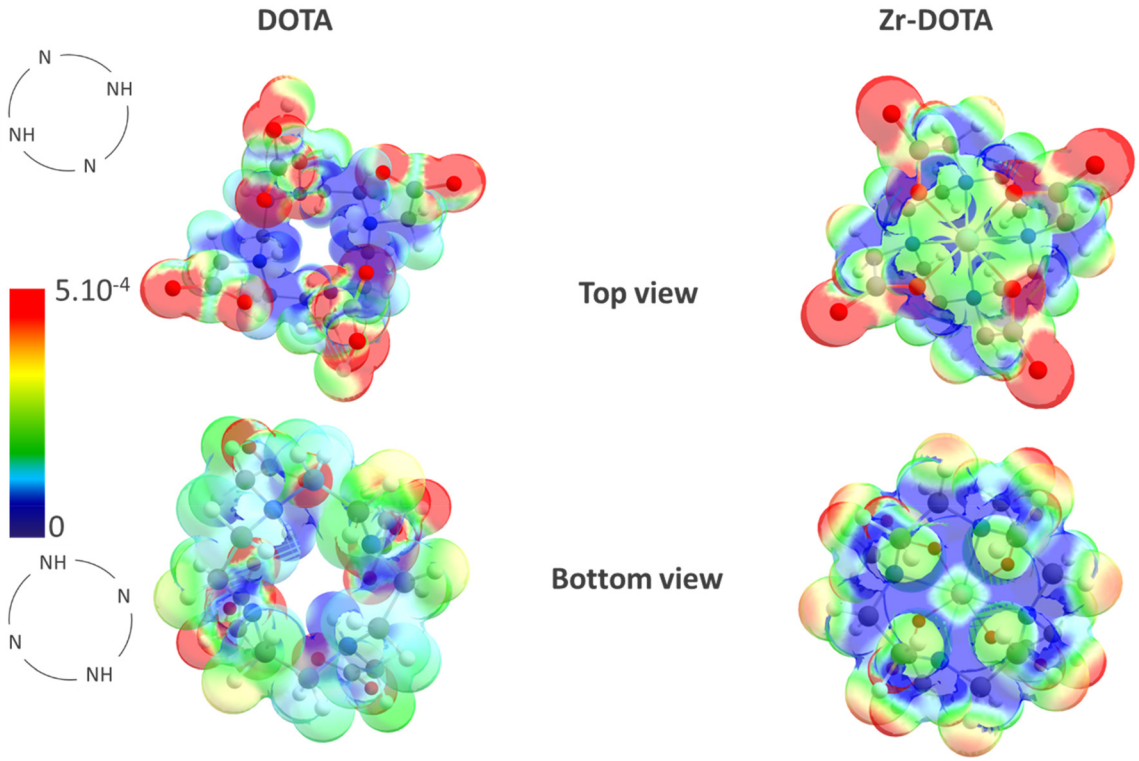

Fig. 9 Radical Fukui function (*R*) calculated for H_4DOTA and Zr–DOTA. The colour scale shows the values of the Fukui function in $e^- Å^{-3}$: low values in blue and high values in red. The top view represents the view with the carboxylates in the foreground, while the bottom view shows the cyclen in the front. The positions of the protonated nitrogens for H_4DOTA are displayed.

Table 6 Radical Fukui indices (f^0) and absolute values of the condensed dual descriptor (CDD) in e for carbons of H_4DOTA and Zr–DOTA

	Atoms	$C_{(COOH)}$	$C_{(COO^-)}$	$C_{(CH_2,\ N\ arm)}$	$C_{(CH_2,\ RN\ arm)}$[a]	$C_{(CH_2,\ cyclen)}$[b]	N	$N_{(RN)}$[a]
H_4DOTA	f^0	0.079	0.003	0.012	0.002	−0.004	0.049	0.003
	|CDD|	0.16	0.006	0.042	0.005	0.013	0.085	0.001
Zr–DOTA	f^0	—	0.011	—	0.002	−0.005	—	0.001
	|CDD|	—	0.017	—	0.01	0.004	—	0.023

[a] R = H^+ or Zr^{4+}. [b] Average values of f^0 and |CDD| for CH_2 of the cyclen.

Finally, if we compare the free ligand and Zr–DOTA, we find that the values obtained for the complex are much lower than those for the free ligand. The highest value for Zr–DOTA is 0.011*e*, while it reaches 0.079*e* for the free ligand.

According to the Fukui indices, Zr–DOTA is more resistant towards radical attack than free DOTA and they have both weaknesses in acetate arms and not in cyclen. Moreover, the Fukui indices f^0 and CDD values of the nitrogen atoms are lowered by the presence of H^+ or Zr^{4+}. This is all consistent with our BDE calculations and ESI-MS results showing that degradation is preferentially located on the DOTA arms for both molecules (the free ligand and ligand involved in the complex). In addition, this confirms that the binding of nitrogen to a cation (H^+ or Zr^{4+}) protects it from radical attack. Using Fukui descriptors, we can also conclude that Zr–DOTA is less prone to degradation than free DOTA.

Conclusion

In this work, we have investigated the radiolytic stability under gamma rays of the DOTA ligand and the Zr–DOTA complex in pure water. DFT calculations supplemented the experimental data and gave an improved understanding of the behaviour of the DOTA and Zr–DOTA solutions after irradiation.

The major degradation products have been identified and the degradation products of the free ligand appear to differ from those of the complex. The free ligand is degraded preferentially by decarboxylation and cleavage of an acetate arm CH_2–COOH, whereas the complex tends to oxidize to form Zr–DOTA[O]. Moreover, the degradation of the DOTA ligand, when complexed with Zr, is significantly less than when the ligand is free in solution, indicating that the metal protects the ligand from degradation. DFT calculations suggest that this

increase in stability is due to the strengthening of the bonds in the presence of metal cations, which become less vulnerable to radical attack. Such a protective effect of the complexation can be expected for any cation if all the acetate arms of the ligands are involved in the cation complexation.

To evaluate the protective effect due to the complexation, further studies should be performed to quantify the DOTA concentration after irradiation. In this work, we investigated the effect of gamma radiation on the DOTA stability. To be more representative of the radiopharmaceutical solutions of ^{89}Zr, this study could be extended to the investigation of the degradation of DOTA in the presence of ^{89}Zr (being β^+ and gamma emitters). Due to the difference in the linear energy transfer between beta and gamma rays, the same degradation products are likely to be observed with a slight difference in their distribution. Also, as DOTA is considered as a good chelator for many radiometals, including α emitters for targeted radiotherapy, it might be interesting to extend this study to the radiolytic stability of DOTA in the presence of α radionuclides such as ^{225}Ac.[86] Alpha emitters have a high linear energy transfer and deposit it within a short range. Moreover, for therapeutic applications, long-lived radionuclides are preferred (a half-life period up to 10 days). Consequently, in the presence of alpha emitters, the radiolytic stability of DOTA could be different.

The influence of a peptide carrier, bonded to DOTA, should also be studied (radiolytic and thermodynamic stabilities) as it is a subject of interest nowadays.[87–89]

Conflicts of interest

There are no conflicts to declare.

Acknowledgements

The authors thank Bertrand Kuhnast and Charles Truillet from the Laboratoire d'Imagerie Biomédicale Multimodale Paris Saclay CEA for the fruitful discussions.

References

1 A. Kasbollah, P. Eu, S. Cowell and P. Deb, *J. Nucl. Med. Technol.*, 2013, **41**, 35–41.
2 M. T. La, V. H. Tran and H.-K. Kim, *Nucl. Med. Mol. Imaging*, 2019, **53**, 115–124.
3 E. C. Dijkers, T. H. O. Munnink, J. G. Kosterink, A. H. Brouwers, P. L. Jager, J. R. de Jong, G. A. van Dongen, C. P. Schroder, M. N. Lub-de Hooge and E. G. de Vries, *Clin. Pharmacol. Ther.*, 2010, **87**, 586–592.
4 J. P. Holland, V. Divilov, N. H. Bander, P. M. Smith-Jones, S. M. Larson and J. S. Lewis, *J. Nucl. Med.*, 2010, **51**, 1293–1300.
5 T. J. Wadas, E. H. Wong, G. R. Weisman and C. J. Anderson, *Chem. Rev.*, 2010, **110**, 2858–2902.
6 L. E. McInnes, S. E. Rudd and P. S. Donnelly, *Coord. Chem. Rev.*, 2017, **352**, 499–516.
7 H. A. Holik, F. M. Ibrahim, A. A. Elaine, B. D. Putra, A. Achmad and A. H. S. Kartamihardja, *Molecules*, 2022, **27**, 3062.
8 M. A. Deri, B. M. Zeglis, L. C. Francesconi and J. S. Lewis, *Nucl. Med. Biol.*, 2013, **40**, 3–14.
9 R. Fu, L. Carroll, G. Yahioglu, E. O. Aboagye and P. W. Miller, *ChemMedChem*, 2018, **13**, 2466–2478.
10 E. T. Sarcan, M. Silindir-Gunay, A. Y. Ozer and N. Hartman, *J. Radioanal. Nucl. Chem.*, 2021, **330**, 15–28.
11 G. W. Severin, J. W. Engle, R. J. Nickles and T. E. Barnhart, *Med. Chem.*, 2011, **7**, 389–394.
12 Y. Zhang, H. Hong and W. Cai, *Curr. Radiopharm.*, 2011, **4**, 131–139.
13 B. Altıparmak Güleç and F. Yurt, *J. Radioanal. Nucl. Chem.*, 2021, **330**, 1–13.
14 E. W. Price and C. Orvig, *Chem. Soc. Rev.*, 2014, **43**, 260–290.
15 N. Herrero Álvarez, D. Bauer, J. Hernández-Gil and J. S. Lewis, *ChemMedChem*, 2021, **16**, 2909–2941.
16 J. R. Dilworth and S. I. Pascu, *Chem. Soc. Rev.*, 2018, **47**, 2554–2571.
17 E. Boros and A. B. Packard, *Chem. Rev.*, 2019, **119**, 870–901.
18 N. B. Bhatt, D. N. Pandya and T. J. Wadas, *Molecules*, 2018, **23**, 638.
19 K. L. Summers, E. K. Sarbisheh, A. Zimmerling, J. J. H. Cotelesage, I. J. Pickering, G. N. George and E. W. Price, *Inorg. Chem.*, 2020, **59**, 17443–17452.
20 T. K. Nayak, K. Garmestani, D. E. Milenic and M. W. Brechbiel, *J. Nucl. Med.*, 2012, **53**, 113–120.
21 M. Audras, L. Berthon, C. Berthon, D. Guillaumont, T. Dumas, M.-C. Illy, N. Martin, I. Zilbermann, Y. Moiseev, Y. Ben-Eliyahu, A. Bettelheim, S. Cammelli, C. Hennig and P. Moisy, *Inorg. Chem.*, 2017, **56**, 12248–12259.
22 C. Tamain, T. Dumas, C. Hennig and P. Guilbaud, *Chem. – Eur. J.*, 2017, **23**, 6864–6875.
23 Z. Baranyai, G. Tircsó and F. Rösch, *Eur. J. Inorg. Chem.*, 2020, **2020**, 36–56.
24 J. L. Domingo, *Reprod. Toxicol.*, 1998, **12**, 499–510.
25 S. Mathur, S. Flora, R. Mathur and S. Dasgupta, *Hum. Exp. Toxicol.*, 1993, **12**, 19–24.
26 D. S. Ma, F. Lu, T. Overstreet, D. E. Milenic and M. W. Brechbiel, *Nucl. Med. Biol.*, 2002, **29**, 91–105.
27 D. N. Pandya, N. Bhatt, H. Yuan, C. S. Day, B. M. Ehrmann, M. Wright, U. Bierbach and T. J. Wadas, *Chem. Sci.*, 2017, **8**, 2309–2314.
28 S. N. Bhattacharyya and K. P. Kundu, *Int. J. Radiat. Phys. Chem.*, 1972, **4**, 31–41.
29 A. P. Toste, *J. Radioanal. Nucl. Chem.*, 2004, **249**, 283–288.
30 N. E. Bibler, *J. Inorg. Nucl. Chem.*, 1972, **34**, 1417–1425.
31 C. A. Zarzana, G. S. Groenewold, B. J. Mincher, S. P. Mezyk, A. Wilden, H. Schmidt, G. Modolo, J. F. Wishart and A. R. Cook, *Solvent Extr. Ion Exch.*, 2015, **33**, 431–447.
32 S. Le Caër, *Water*, 2011, **3**, 235–253.

33 A. H. Samuel and J. L. Magee, *J. Chem. Phys.*, 1953, **21**, 1080–1087.
34 W. G. Burns and H. E. Sims, *J. Chem. Soc., Faraday Trans. 1*, 1981, **77**, 2803–2813.
35 B. Pastina and J. A. LaVerne, *J. Phys. Chem. A*, 1999, **103**, 1592–1597.
36 V. Fiegel, C. Berthon, A. Costagliola, G. Blain, J. Vandenborre, J. Vermeulen, G. Saint-Louis, L. Guerin, T. Sauvage, M. Fattahi-Vanani, L. Venault and L. Berthon, *Radiat. Phys. Chem.*, 2019, **165**, 108409.
37 E. Avraham, D. Meyerstein, A. Lerner, G. Yardeni, S. Pevzner, I. Zilbermann, P. Moisy, E. Maimon and I. Popivker, *Free Radicals Biol. Med.*, 2022, **180**, 134–142.
38 C. C. Barros, C. D. Pilgrim, A. R. Cook, S. P. Mezyk, T. S. Grimes and G. P. Horne, *Phys. Chem. Chem. Phys.*, 2021, **23**, 24589–24597.
39 T. Toigawa, D. R. Peterman, D. S. Meeker, T. S. Grimes, P. R. Zalupski, S. P. Mezyk, A. R. Cook, S. Yamashita, Y. Kumagai, T. Matsumura and G. P. Horne, *Phys. Chem. Chem. Phys.*, 2021, **23**, 1343–1351.
40 A. Kimberlin, G. Saint-Louis, D. Guillaumont, B. Camès, P. Guilbaud and L. Berthon, *Phys. Chem. Chem. Phys.*, 2022, **24**, 9213–9228.
41 B. K. Sharma and R. Gupta, *Radiat. Eff.*, 1981, **57**, 149–154.
42 G. V. Buxton and R. M. Sellers, *Coord. Chem. Rev.*, 1977, **22**, 195–274.
43 S. N. Bhattacharyya and K. P. Kundu, *Int. J. Radiat. Phys. Chem.*, 1971, **3**, 1–10.
44 K. P. Kundu and N. Matsuura, *Int. J. Radiat. Phys. Chem.*, 1975, **7**, 565–571.
45 G. R. Buettner, T. P. Doherty and L. K. Patterson, *FEBS Lett.*, 1983, **158**, 143–146.
46 Y. A. Ilan and G. Czapski, *Biochim. Biophys. Acta, Gen. Subj.*, 1977, **498**, 386–394.
47 B. K. Sharma and R. Gupta, *Radiat. Phys. Chem.*, 1984, **24**, 233–237.
48 M. M. Khater, I. M. Kenawi, A. M. Atwa and M. B. Hafez, *J. Radioanal. Nucl. Chem.*, 1987, **111**, 17–26.
49 M. B. Hafez, H. Rouhdy and N. Hafez, *J. Radioanal. Chem.*, 1978, **43**, 121–129.
50 S. N. Bhattacharyya and E. V. Srisankar, *Int. J. Radiat. Phys. Chem.*, 1976, **8**, 667–671.
51 A. Kimberlin, D. Guillaumont, S. Arpigny, B. Camès, P. Guilbaud, G. Saint-Louis, H. Galán and L. Berthon, *New J. Chem.*, 2021, **45**, 12479–12493.
52 P. I. Matveev, A. A. Mitrofanov, V. G. Petrov, S. S. Zhokhov, A. A. Smirnova, Y. A. Ustynyuk and S. N. Kalmykov, *RSC Adv.*, 2017, **7**, 55441–55449.
53 A. Smirnova, A. Mitrofanov, P. Matveev, T. Baygildiev and V. Petrov, *Phys. Chem. Chem. Phys.*, 2020, **22**, 14992–14997.
54 T. Koubský, J. Fojtíková and L. Kalvoda, *Prog. Nucl. Energy*, 2017, **94**, 208–215.
55 T. Koubský and J. Luštinec, *J. Radioanal. Nucl. Chem.*, 2018, **318**, 2407–2413.
56 F. H. Attix, W. C. Roesch and E. Tochilin, *Radiation dosimetry*, Academic Press, New York [etc.], 1966.
57 C. Truillet, E. Thomas, F. Lux, L. T. Huynh, O. Tillement and M. J. Evans, *Mol. Pharmaceutics*, 2016, **13**, 2596–2601.
58 M. J. Frisch, G. W. Trucks, H. B. Schlegel, G. E. Scuseria, M. A. Robb, J. R. Cheeseman, G. Scalmani, V. Barone, G. A. Petersson and H. Nakatsuji, *Gaussian 16*, Gaussian, Inc., Wallingford, CT, 2016.
59 D. Andrae, U. Häußermann, M. Dolg, H. Stoll and H. Preuß, *Theor. Chim. Acta*, 1990, **77**, 123–141.
60 A. D. Becke, *J. Chem. Phys.*, 1993, **98**, 5648–5652.
61 J. P. Perdew, *Phys. Rev. B: Condens. Matter Mater. Phys.*, 1986, **33**, 8822–8824.
62 Y. Feng, L. Liu, J.-T. Wang, H. Huang and Q.-X. Guo, *J. Chem. Inf. Comput. Sci.*, 2003, **43**, 2005–2013.
63 C. Qi, Q.-H. Lin, Y.-Y. Li, S.-P. Pang and R.-B. Zhang, *J. Mol. Struct.: THEOCHEM*, 2010, **961**, 97–100.
64 H. Zeng, J. Zhao and X. Xiao, *Chin. Phys. B*, 2013, **22**, 023301.
65 R. G. Parr and W. Yang, *J. Am. Chem. Soc.*, 1984, **106**, 4049–4050.
66 C. Morell, A. Grand and A. Toro-Labbé, *J. Phys. Chem. A*, 2005, **109**, 205–212.
67 C. Morell, A. Grand and A. Toro-Labbé, *Chem. Phys. Lett.*, 2006, **425**, 342–346.
68 A. D. Becke, *J. Chem. Phys.*, 1993, **98**, 1372–1377.
69 C. Lee, W. Yang and R. G. Parr, *Phys. Rev. B: Condens. Matter Mater. Phys.*, 1988, **37**, 785–789.
70 J. Tomasi, B. Mennucci and R. Cammi, *Chem. Rev.*, 2005, **105**, 2999–3094.
71 E. Glendening, A. Reed, J. Carpenter and F. Weinhold, *NBO 3.1*.
72 D. Parker, K. Pulukkody, F. C. Smith, A. Batsanov and J. A. K. Howard, *J. Chem. Soc., Dalton Trans.*, 1994, 689–693.
73 B. J. Mincher, G. Modolo and S. P. Mezyk, *Solvent Extr. Ion Exch.*, 2009, **27**, 1–25.
74 B. J. Mincher and R. D. Curry, *Appl. Radiat. Isot.*, 2000, **52**, 189–193.
75 M. Audras, L. Berthon, N. Martin, N. Zorz and Ph. Moisy, *J. Radioanal. Nucl. Chem.*, 2015, **303**, 1897–1909.
76 Y. Moiseev, Y. Ben-Eliyahu, M. Audras, L. Berthon, P. Moisy, A. Bettelheim and I. Zilbermann, *J. Coord. Chem.*, 2016, **69**, 2895–2907.
77 G. P. Horne, A. Wilden, S. P. Mezyk, L. Twight, M. Hupert, A. Stärk, W. Verboom, B. J. Mincher and G. Modolo, *Dalton Trans.*, 2019, **48**, 17005–17013.
78 J. A. Drader, N. Boubals, B. Camès, D. Guillaumont, P. Guilbaud, G. Saint-Louis and L. Berthon, *Dalton Trans.*, 2018, **47**, 251–263.
79 J. Drader, G. Saint-Louis, J. M. Muller, M.-C. Charbonnel, P. Guilbaud, L. Berthon, K. M. Roscioli-Johnson, C. A. Zarzana, C. Rae, G. S. Groenewold, B. J. Mincher, S. P. Mezyk, K. McCann, S. G. Boyes and J. Braley, *Solvent Extr. Ion Exch.*, 2017, **35**, 480–495.
80 J. Moreau, E. Guillon, J.-C. Pierrard, J. Rimbault, M. Port and M. Aplincourt, *Chem. – Eur. J.*, 2004, **10**, 5218–5232.
81 J. F. Desreux, E. Merciny and M. F. Loncin, *Inorg. Chem.*, 1981, **20**, 987–991.

82 L. Burai, I. Fábián, R. Király, E. Szilágyi and E. Brücher, *J. Chem. Soc., Dalton Trans.*, 1998, 243–248.
83 J. Hioe, D. Šakić, V. Vrček and H. Zipse, *Org. Biomol. Chem.*, 2015, **13**, 157–169.
84 D. Kaur and R. P. Kaur, *J. Mol. Struct.: THEOCHEM*, 2008, **858**, 94–100.
85 D. Šakić and H. Zipse, *Adv. Synth. Catal.*, 2016, **358**, 3983–3991.
86 A. Morgenstern, C. Apostolidis, C. Kratochwil, M. Sathekge, L. Krolicki and F. Bruchertseifer, *Curr. Radiopharm.*, 2018, **11**, 200–208.
87 V.-L. Tran, F. Lux, N. Tournier, B. Jego, X. Maître, M. Anisorac, C. Comtat, S. Jan, K. Selmeczi, M. J. Evans, O. Tillement, B. Kuhnast and C. Truillet, *Adv. Healthcare Mater.*, 2021, **10**, 2100656.
88 F. Lux, V. L. Tran, E. Thomas, S. Dufort, F. Rossetti, M. Martini, C. Truillet, T. Doussineau, G. Bort, F. Denat, F. Boschetti, G. Angelovski, A. Detappe, Y. Crémillieux, N. Mignet, B.-T. Doan, B. Larrat, S. Meriaux, E. Barbier, S. Roux, P. Fries, A. Müller, M.-C. Abadjian, C. Anderson, E. Canet-Soulas, P. Bouziotis, M. Barberi-Heyob, C. Frochot, C. Verry, J. Balosso, M. Evans, J. Sidi-Boumedine, M. Janier, K. Butterworth, S. McMahon, K. Prise, M.-T. Aloy, D. Ardail, C. Rodriguez-Lafrasse, E. Porcel, S. Lacombe, R. Berbeco, A. Allouch, J.-L. Perfettini, C. Chargari, E. Deutsch, G. Le Duc and O. Tillement, *Br. J. Radiol.*, 2018, **92**, 20180365.
89 P. Fries, D. Morr, A. Müller, F. Lux, O. Tillement, A. Massmann, R. Seidel, T. Schäfer, M. D. Menger, G. Schneider and A. Bücker, *RoFo*, 2015, **187**, 1108–1115.